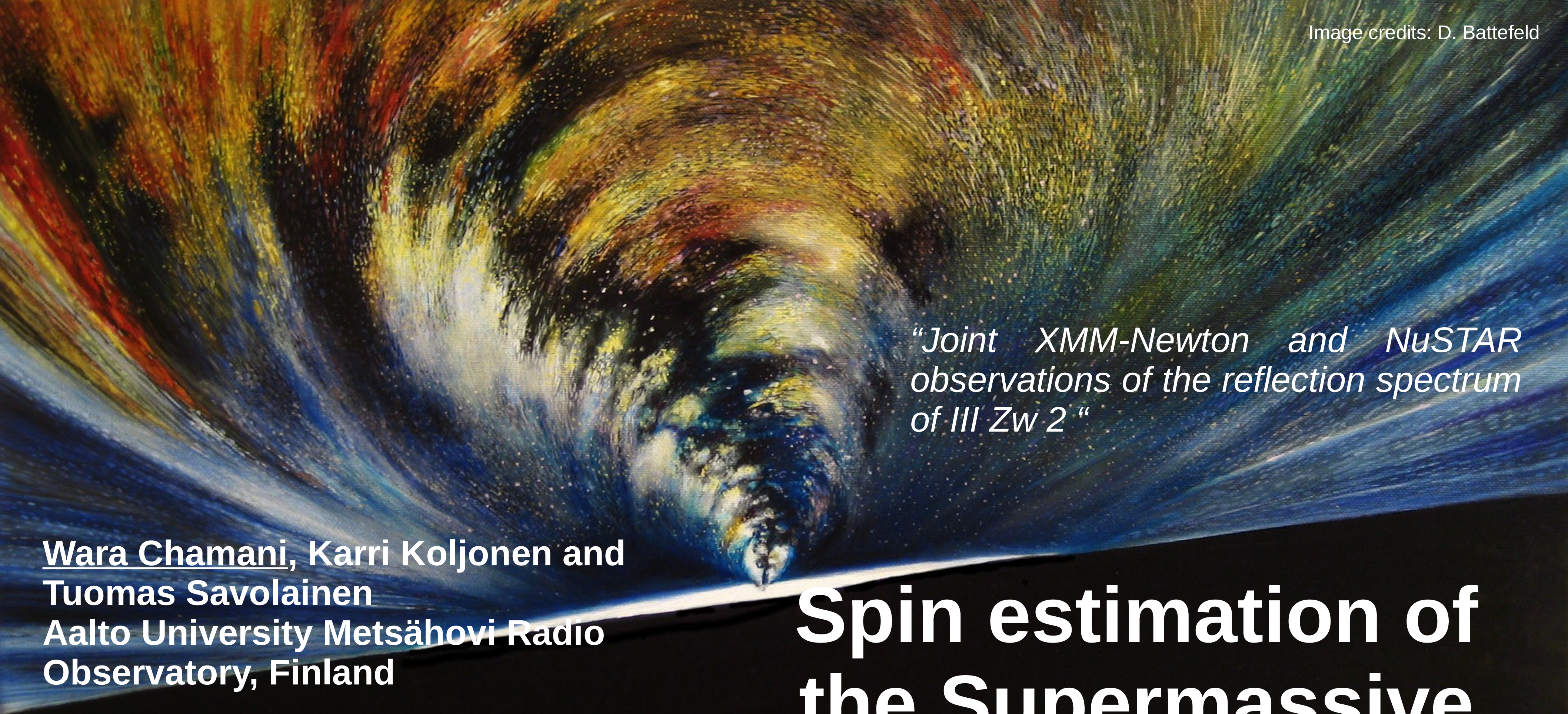

Image credits: D. Battefeld

"Joint XMM-Newton and NuSTAR observations of the reflection spectrum of III Zw 2 "

Spin estimation of the Supermassive Black Hole of III Zw 2

Wara Chamani, Karri Koljonen and Tuomas Savolainen
Aalto University Metsähovi Radio Observatory, Finland

AGN Jet Workshop January 2020
Tohoku University, Sendai

Black hole spin observations

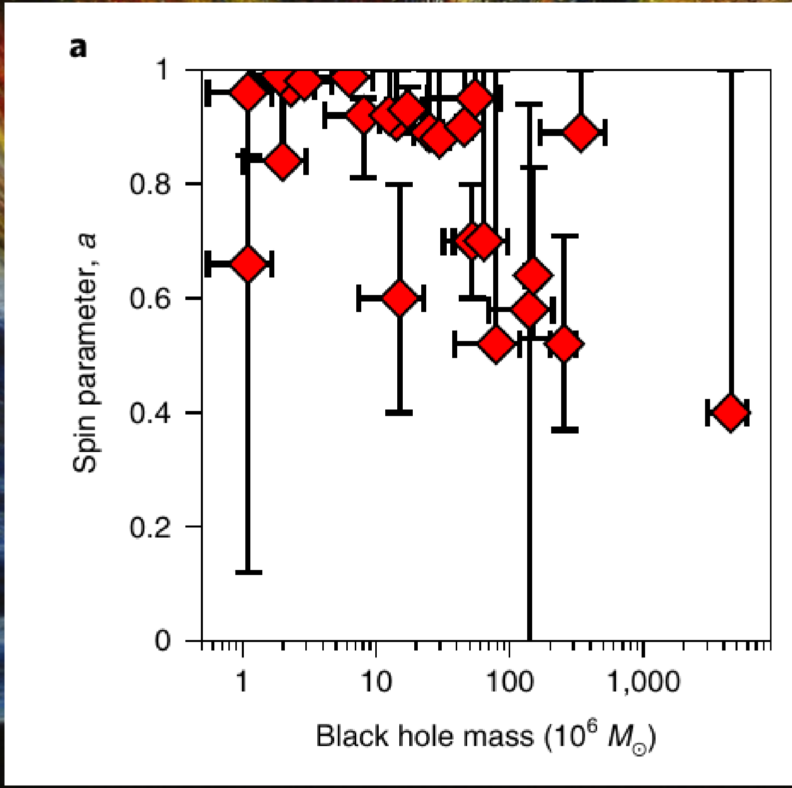

Reynolds 2019.

→ 22 robust spin values measured using X-ray reflection method.

→ No Spin vs BH mass correlation.

Motivation of this work

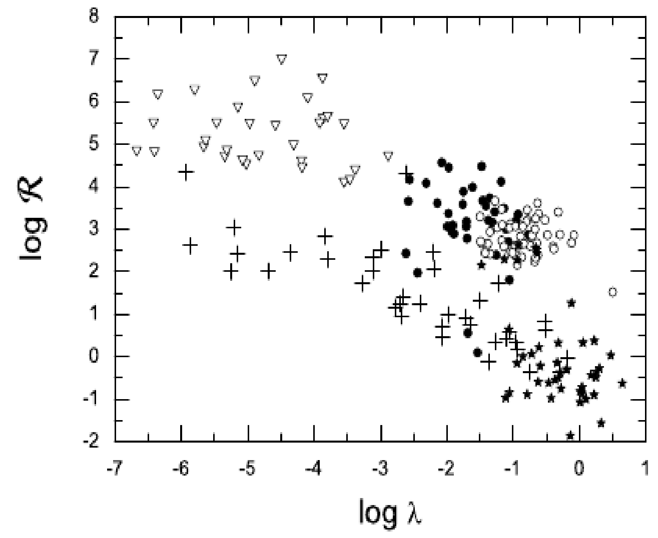

FIG. 3.—Radio loudness $\mathcal{R}$ vs. Eddington ratio λ. BLRGs are marked by filled circles, radio loud quasars by open circles, Seyfert galaxies and LINERs by crosses, FR I radio galaxies by open triangles, and PG quasars by filled stars.

Sikora+2007.

→ A wide radio-loudness (*R*) distribution in AGN.
→ at leat 4 orders of magnitude of accretion rate difference!.

What creates a powerful black hole jet?
"Spin paradigm" → attempts to explain the wide *R* (Wilson & Colbert 1995, Blandford 1999, Sikora+2007, Tschekhovskoy+2010).

Powerful jet → High black hole spin?
Weak jet → Low black hole spin?

Which other parameter can dominate besides the spin?

Motivation of this work

Magnetic flux threading the black hole → that launch powerfull jets.
"Magnetic flux paradigm" → may explain the *R* dichotomy (Sikora & Begelman2007).

Magnetically Arrested Disk (MAD) (Narayan + 2003; Tchekhovskoy +2011; McKinney + 2012) explains the powerful jets.

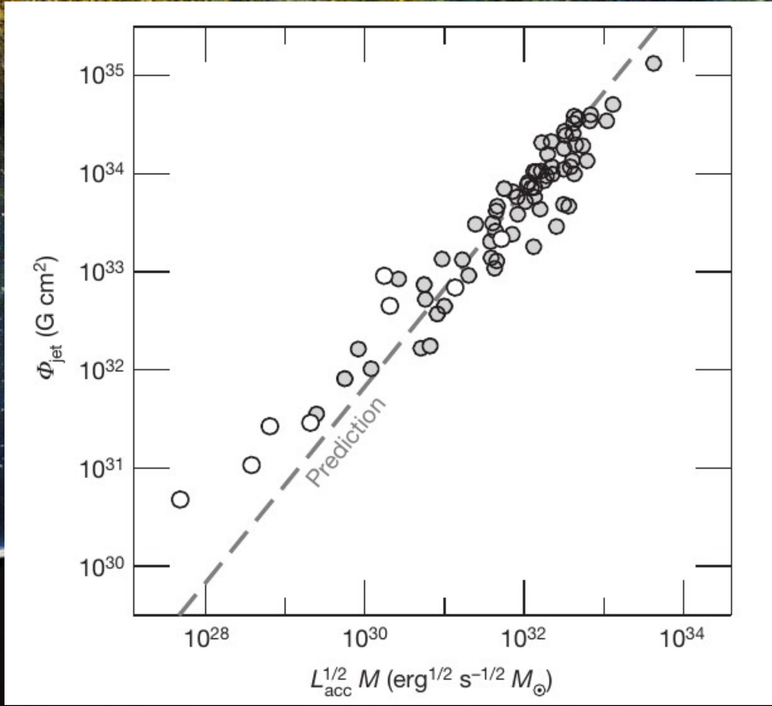

Jet magnetic flux versus $L_{acc}M_{BH}$ for FSRL+RG+Low Luminosity Radio Loud AGN. Solid line is the MAD prediction. (Zamaninasab+2014)

Motivation of this work

Magnetic flux threading the black hole → that launch powerfull jets.
"Magnetic flux paradigm" → could explain the *R* dichotomy (Sikora & Begelman2007)

Magnetically Arrested Disk (MAD) (Narayan + 2003; Tchekhovskoy +2011; McKinney + 2012)
Tested in a sample of powerful jets.

Physical parameters MAD model: **BH spin** (X-rays) + **Jet's Magnetic field flux** (VLBI).

Our sample (weak jets) (1<*R*<200): E1821+643,
III Zw 2 (presented in this conference), PG 2209+184 and PG 1309+355.

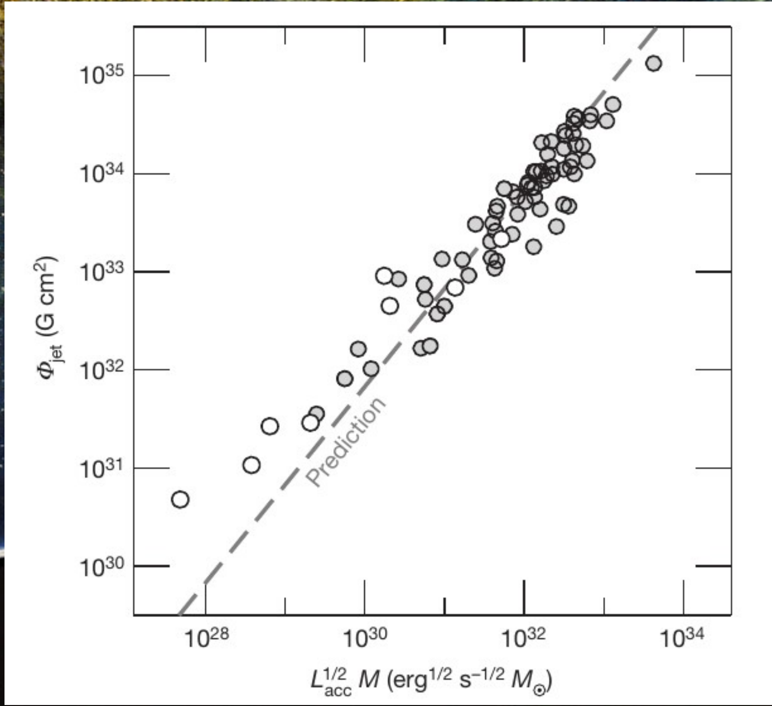

Jet magnetic flux versus $L_{acc}M_{BH}$ for FSRL+RG+Low Luminosity Radio Loud AGN. Solid line is the MAD prediction. (Zamaninasab+2014)

The nature of III Zw 2.

- A RIQ, it certainly emits radiation from radio to gamma-ray wavelengths.
- Highly variable in radio band emissions.
- Li+2010: Quasi periodic activity. Outburst period ~ 5 years at 22 and 37 GHz. This might be due to the rotation of the helix in the jet.

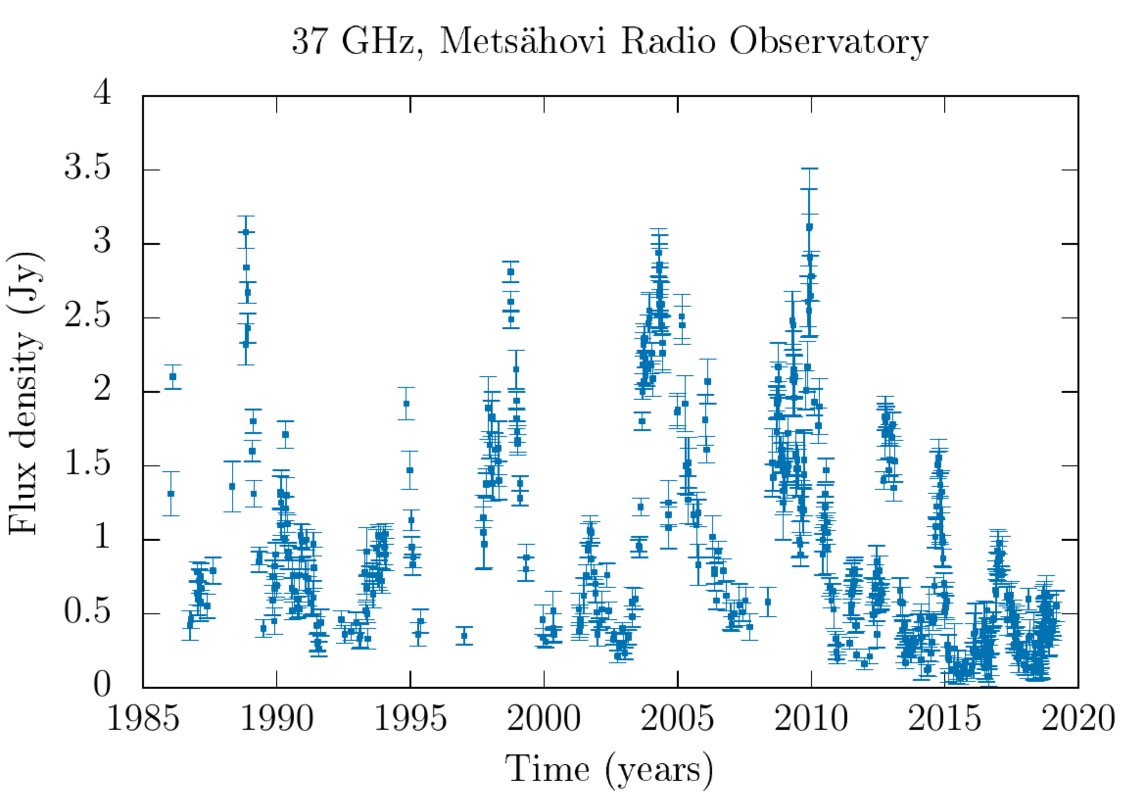

VLBI observations of III Zw 2

It has a compact radio core.

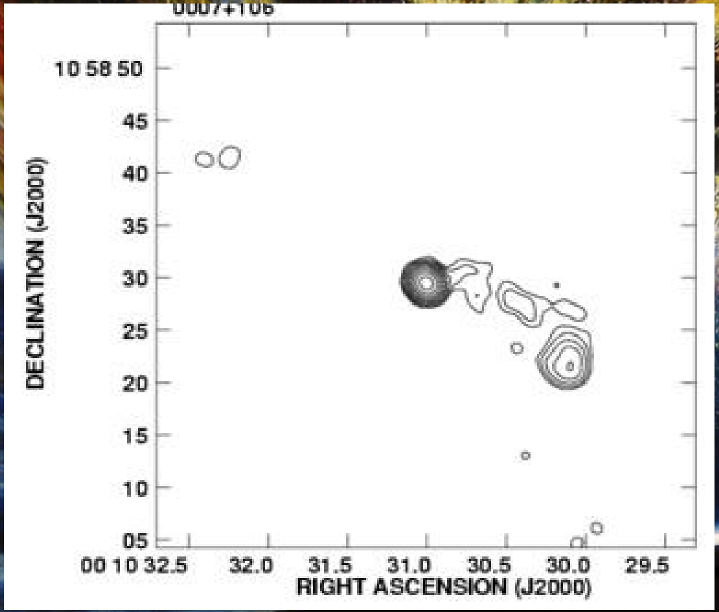

VLA-A configuration 1.4 GHz image in the MOJAVE sample (Cooper+2017).

Core dominated flat radio spectrum

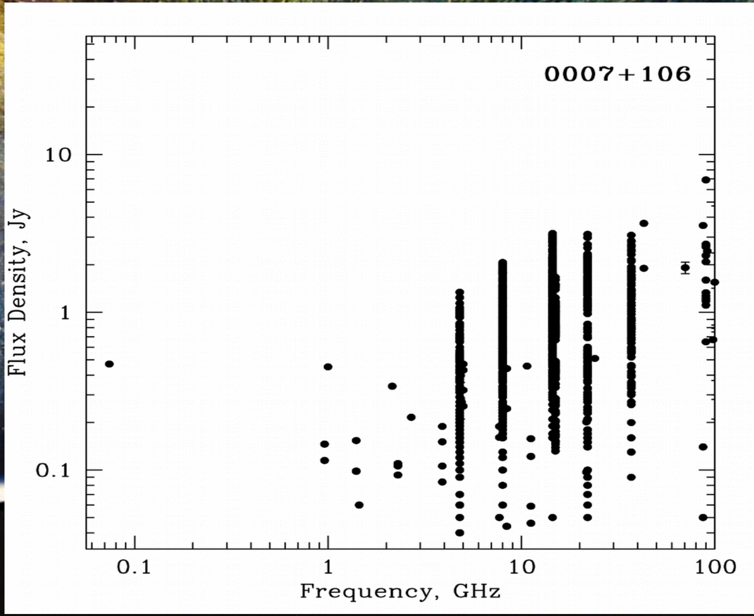

MOJAVE archive.

- A jetted source with a apparent superluminal motion :1.58±0.29c (Lister et al. 2019).
- Maximum jet's viewing angle: 41^{o} (Brunthaler+2000).

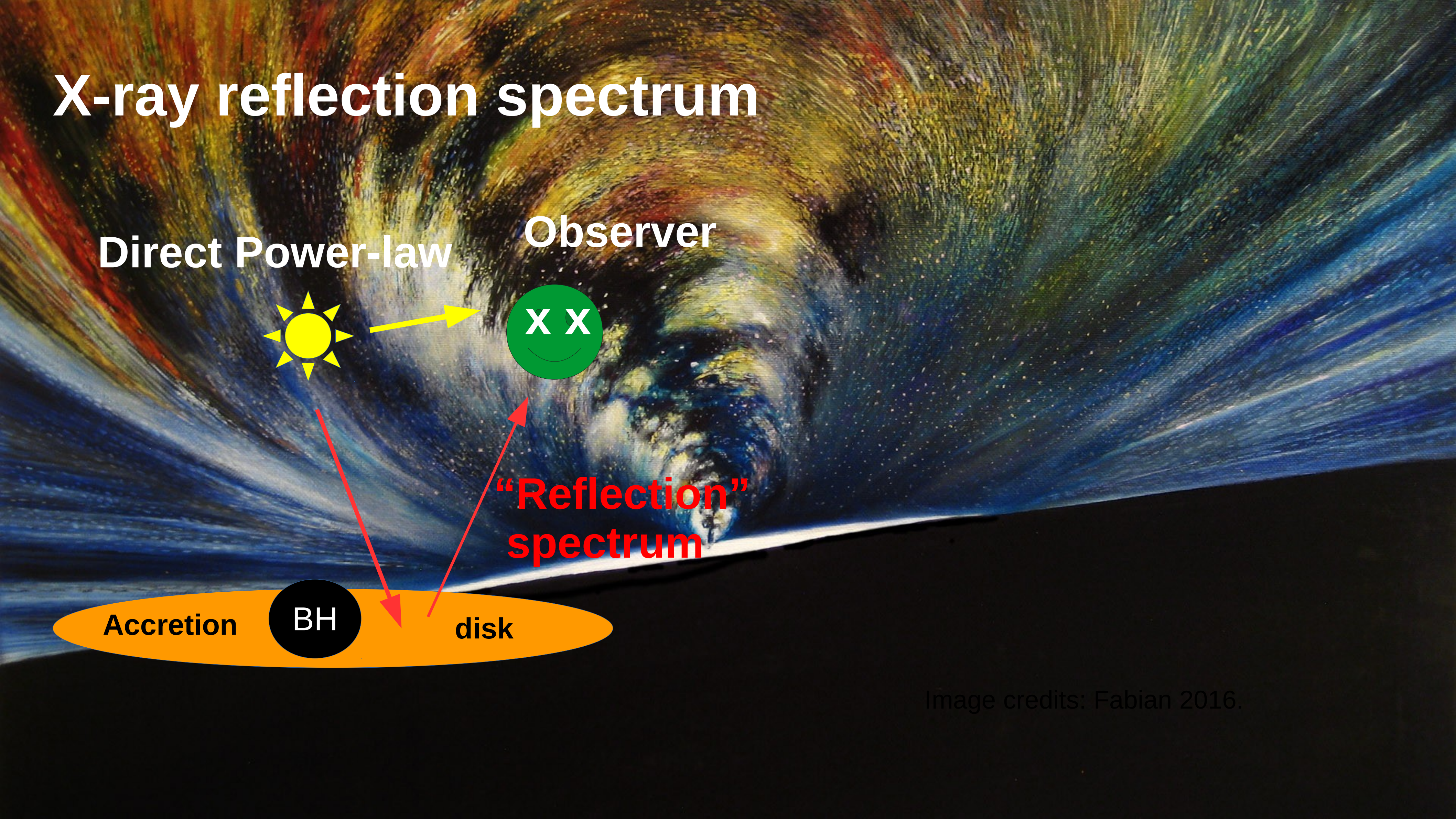
X-ray reflection spectrum
Direct Power-law
Observer
X X
"Reflection" spectrum
Accretion
BH
disk
Image credits: Fabian 2016.

X-ray reflection spectrum

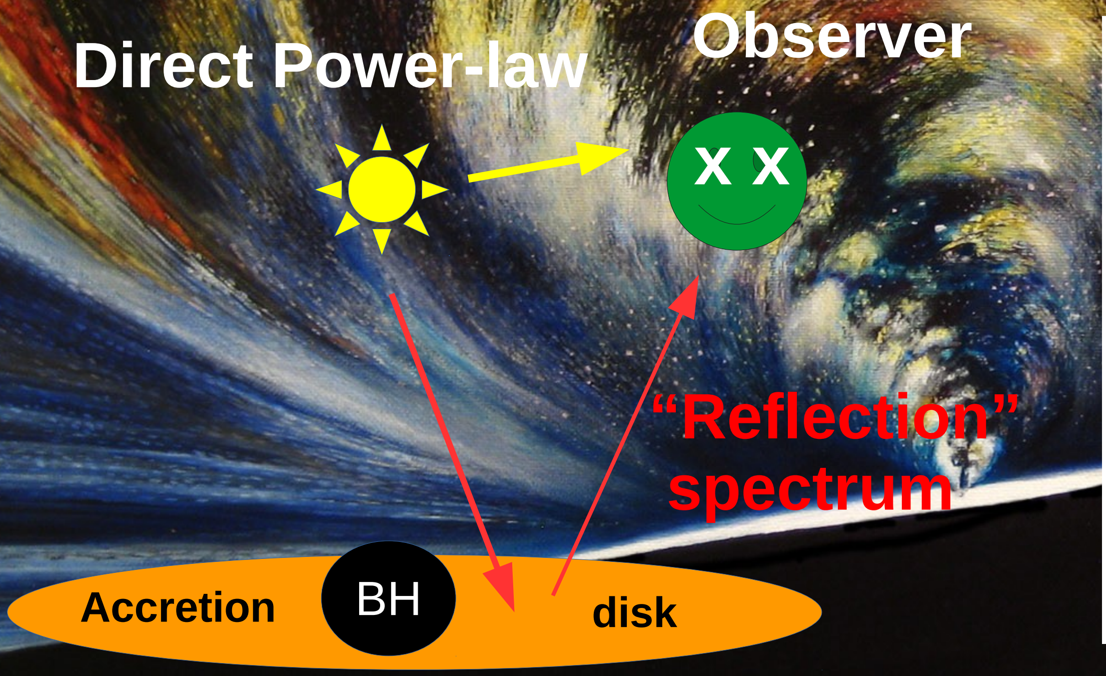

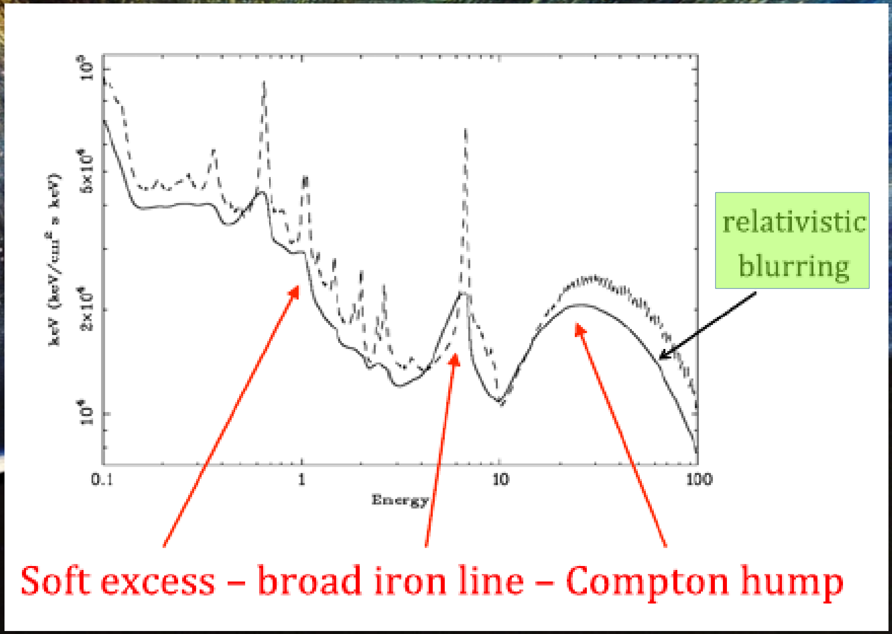

Credits: Fabian 2016.

Image credits: Fabian 2016.

Black hole spin, FeK line at 6.4 keV

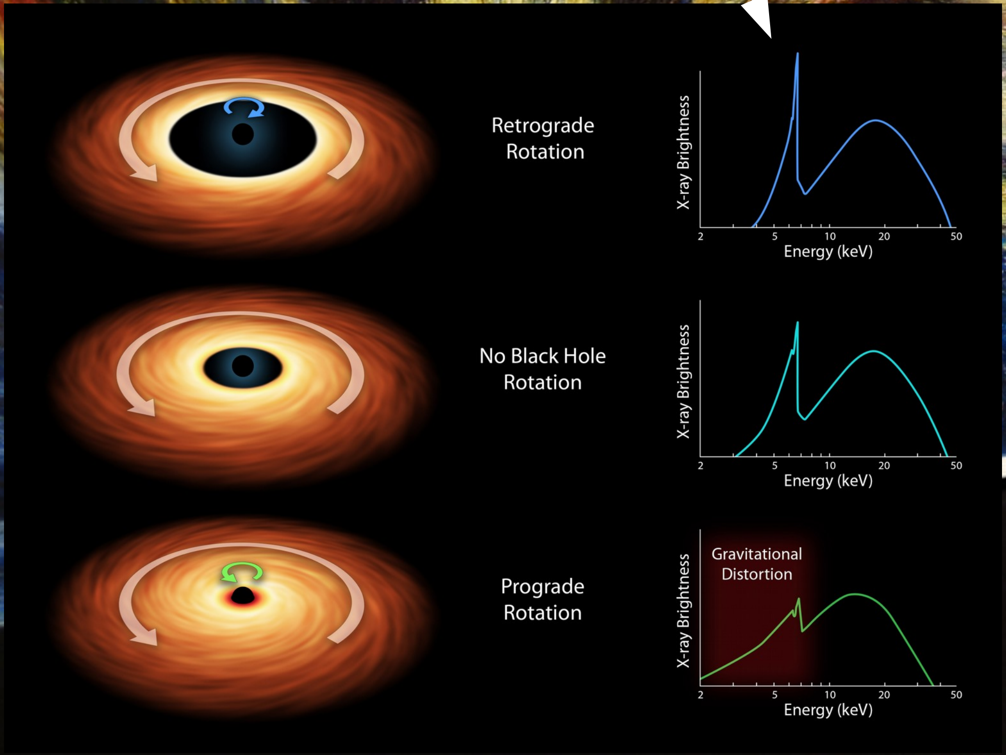

Image taken from NASA pictures.

Black hole spin, FeK line at 6.4 keV

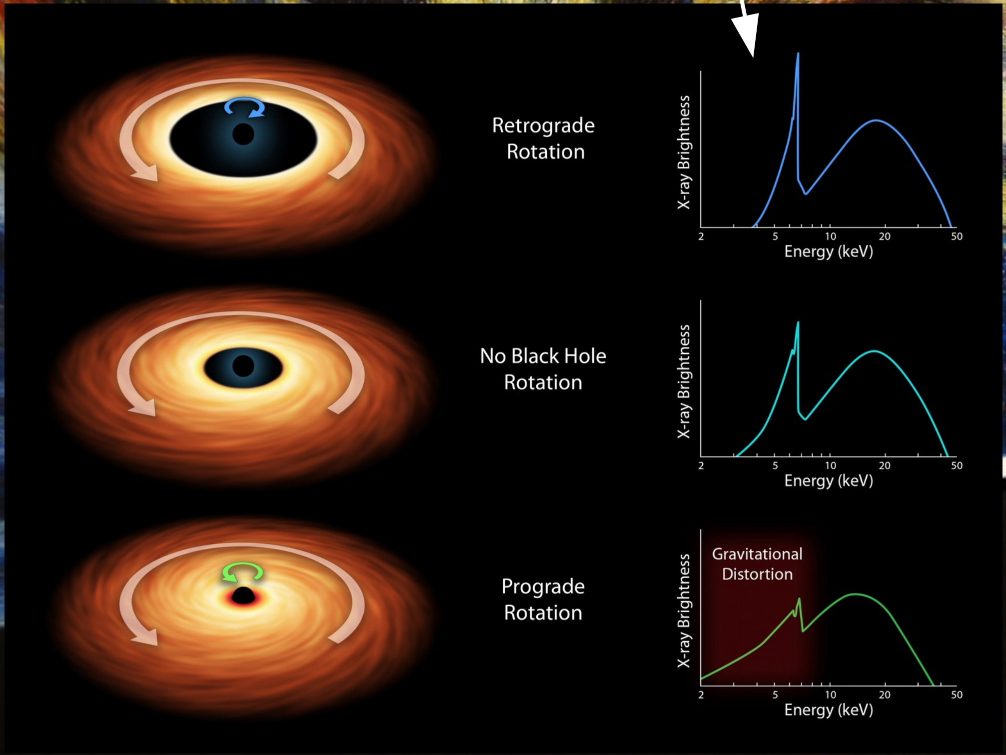

Image taken from NASA pictures.

X-ray Reflection spectrum

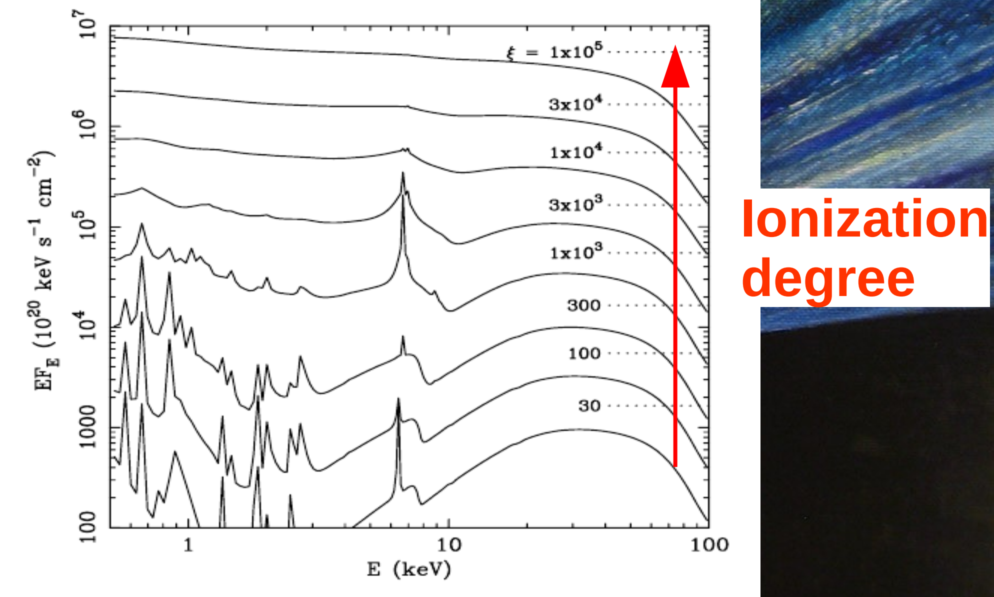

FIG. 2.—Reflection spectra from ionized matter for various values of the ionization parameter ξ. The dotted lines show the level of the illuminating power-law continuum for each value of ξ.

Credits: Fabian+2000.

Simultaneous X-ray satellite observations of III Zw 2

- **Our observations were made on 11.12.2017**

XMM-Newton
11.94 hours of exposure

\+

NuSTAR
26.03 hours of exposure

= Broad Band energy X- ray observations (0.2 – 70 keV)

- Data reduction: running different pipelines and checking of pileups.
- Data analysis with the ISIS (Interactive Spectral Interpretation System) package.

Reflection spectrum of III Zw 2

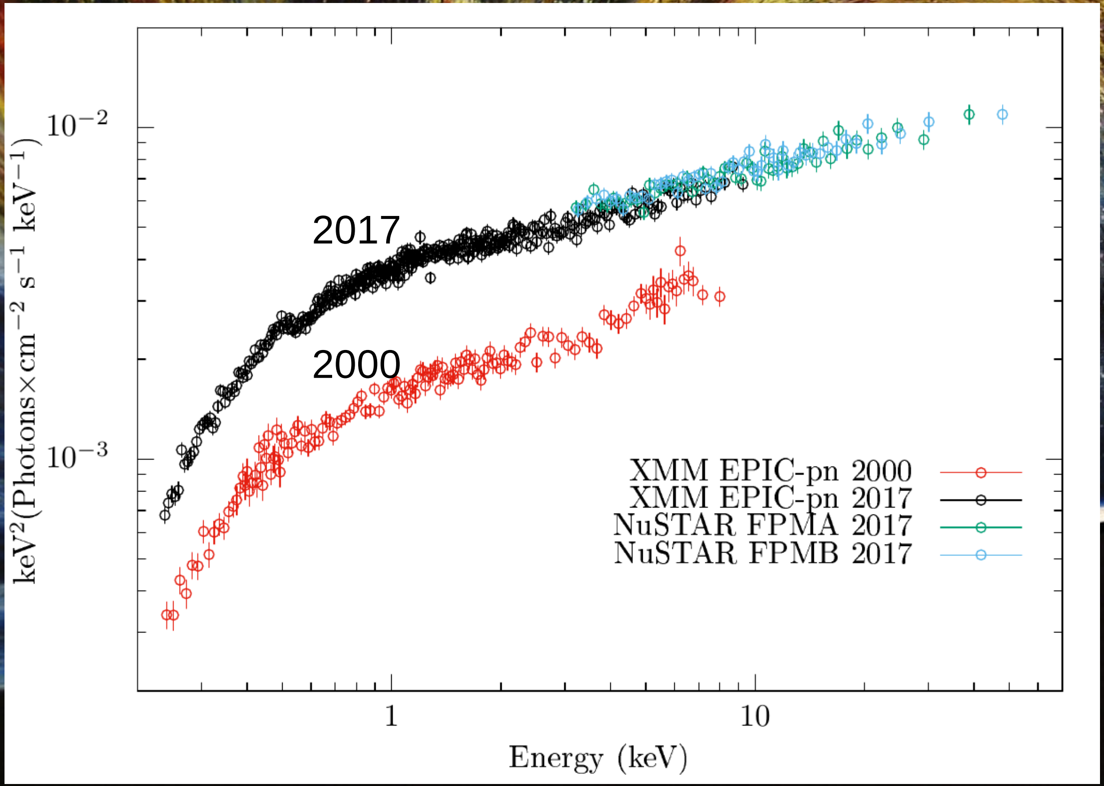

- Our observations taken in 2017 gathered more X-ray data.
- Hard X-ray detections > 10keV.
- XMM archival data of 2000.
- X-ray flux increases after 17 years by a factor of ~2.

Search for the presence of FeK line

Residuals of Power Law fit to the spectra

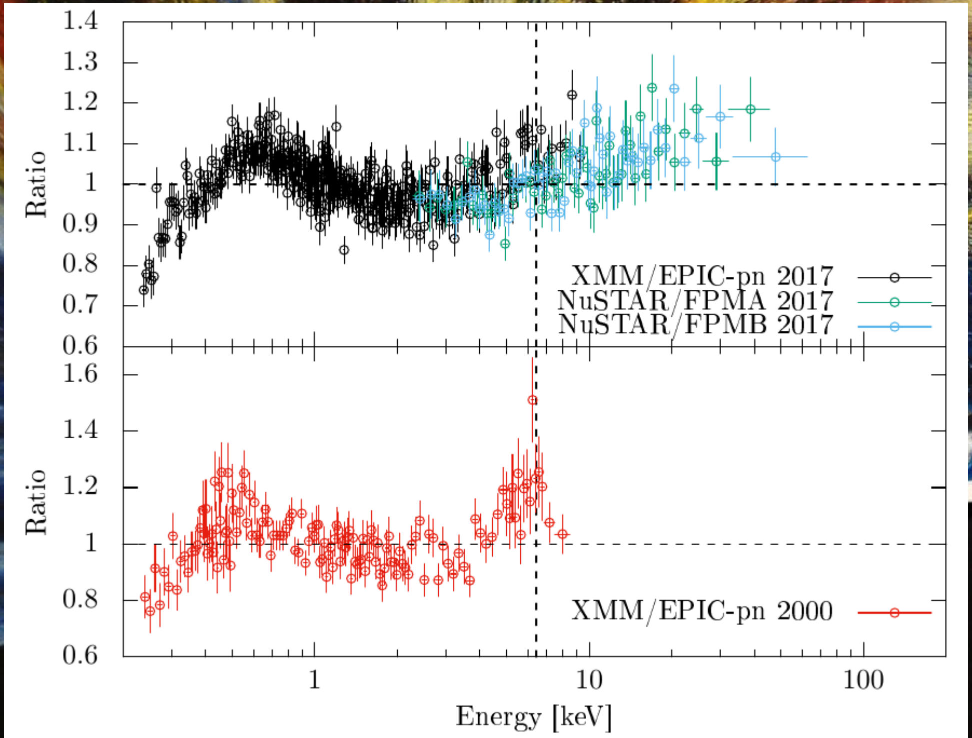

Energy of the FeK line: 6.4 keV

Search for the presence of FeK line

Residuals of Power Law (PL) fit to the spectra

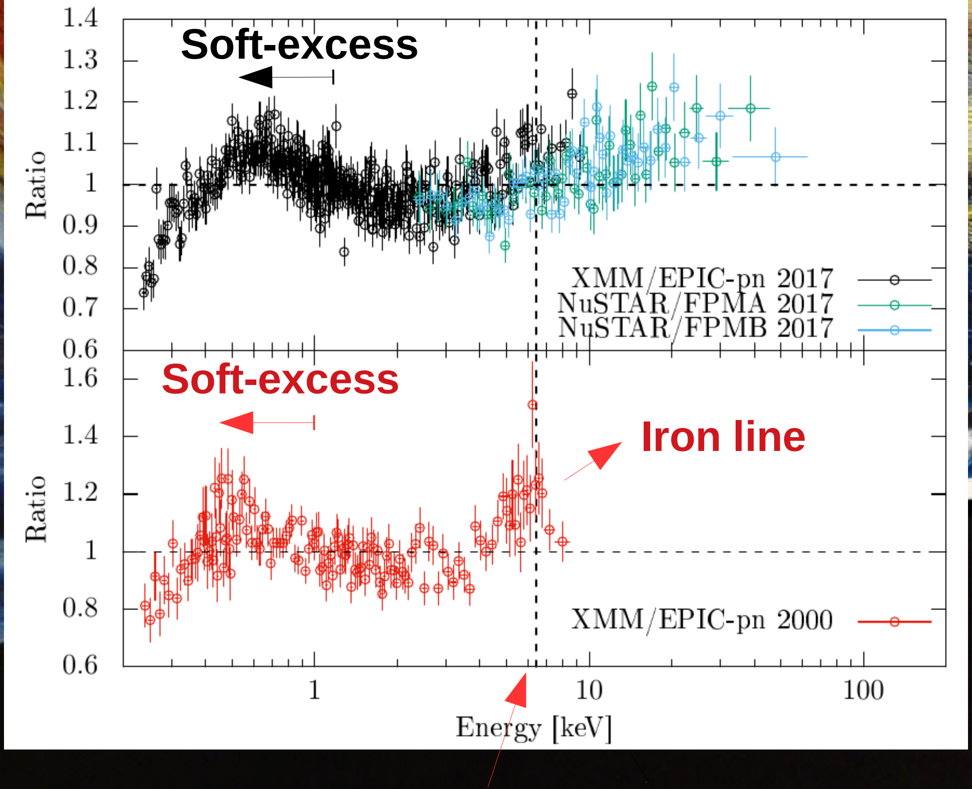

Energy of the FeK line: 6.4 keV

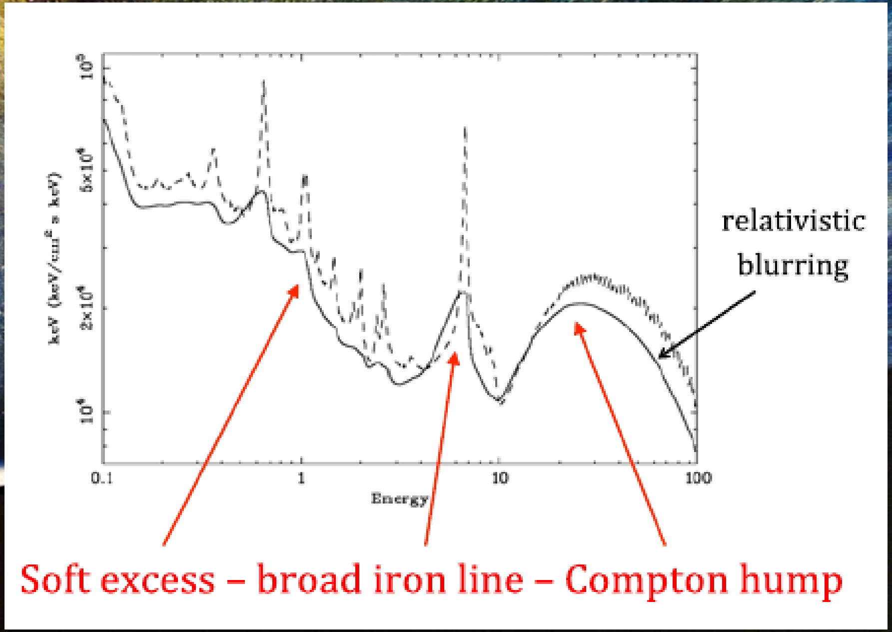

FeK line detection (Salvi+2002, Piconcelli+2005, Jiménez-Bailón+2005).

Search for the presence of FeK line

Residuals of a Power law + Black Body fit

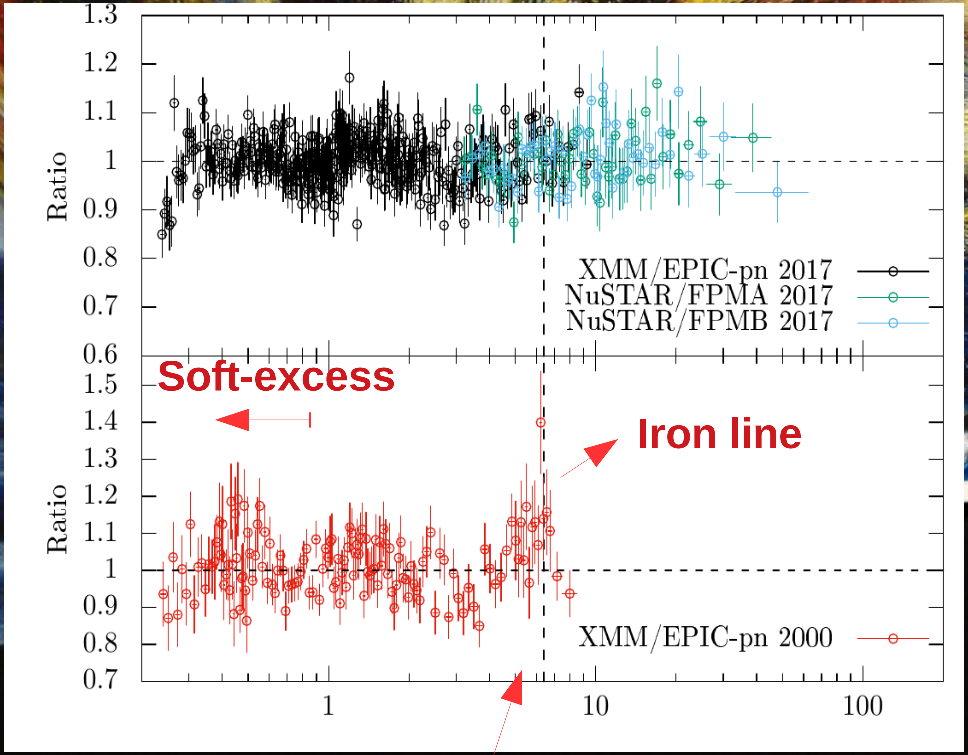

Energy of the FeK line: 6.4 keV

- A good improvement on the fitting of the 2017-soft excess.
- Soft-excess still visible on the 2000 data.
- Black body temperatures: 136-144 eV >> standard disk temperature (~10 eV).
- Which mechanism is driving the soft-excess?

X-ray relativistic reflection models

RELXILL code =

XILLVER code (reflected spectrum)

+

RELLINE code (relativistic blurring effects)

RELXILL model (Garcia +2014).

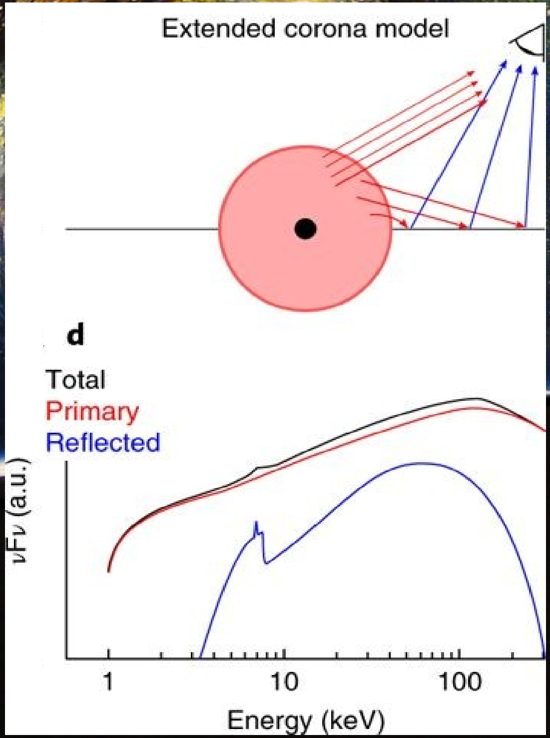

RELXILL-LP (Lamp-post) model (Dauser+2013).

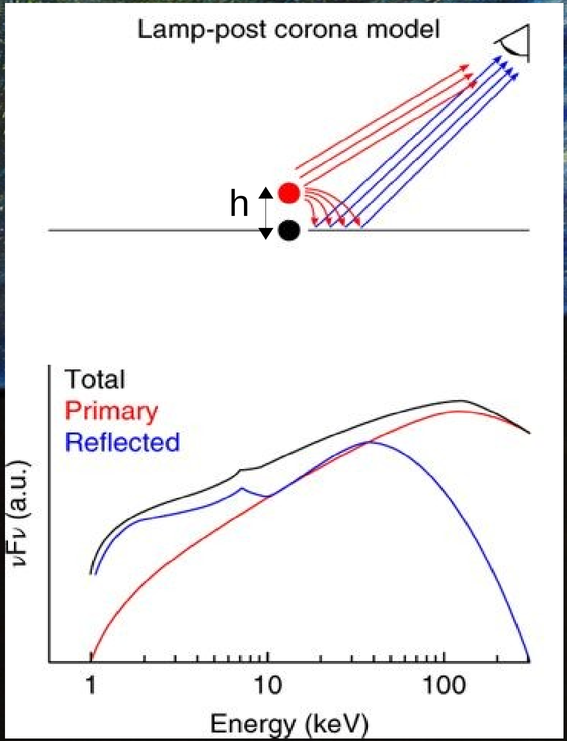

Images credits: Chauvin+2018

X-ray relativistic reflection models

Physical parameters:

- Spin: a
- Reflection fraction: R
- Disk Inclination: θ
- Ionization parameter: ξ
- Iron Abundance: A_{FE}
- Power Law photon index: Γ

RELXILL model (Garcia +2014).

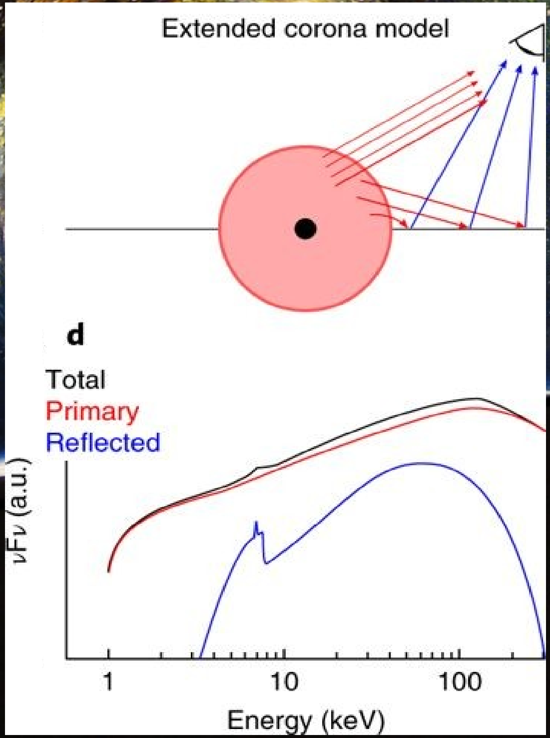

RELXILL-LP (Lamp-post) model (Dauser+2013).

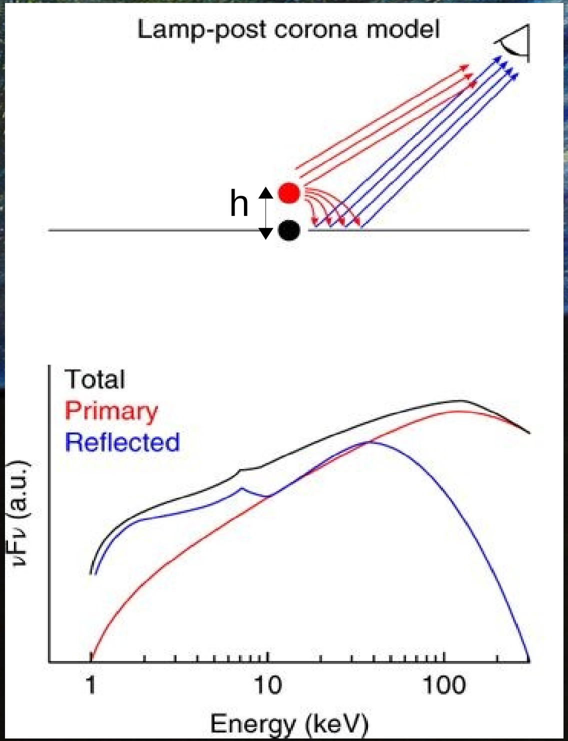

Images credits: Chauvin+2018

Fitting the data with RELXILL

Spin '*a*' and other parameters obtained with a *joint*-fit

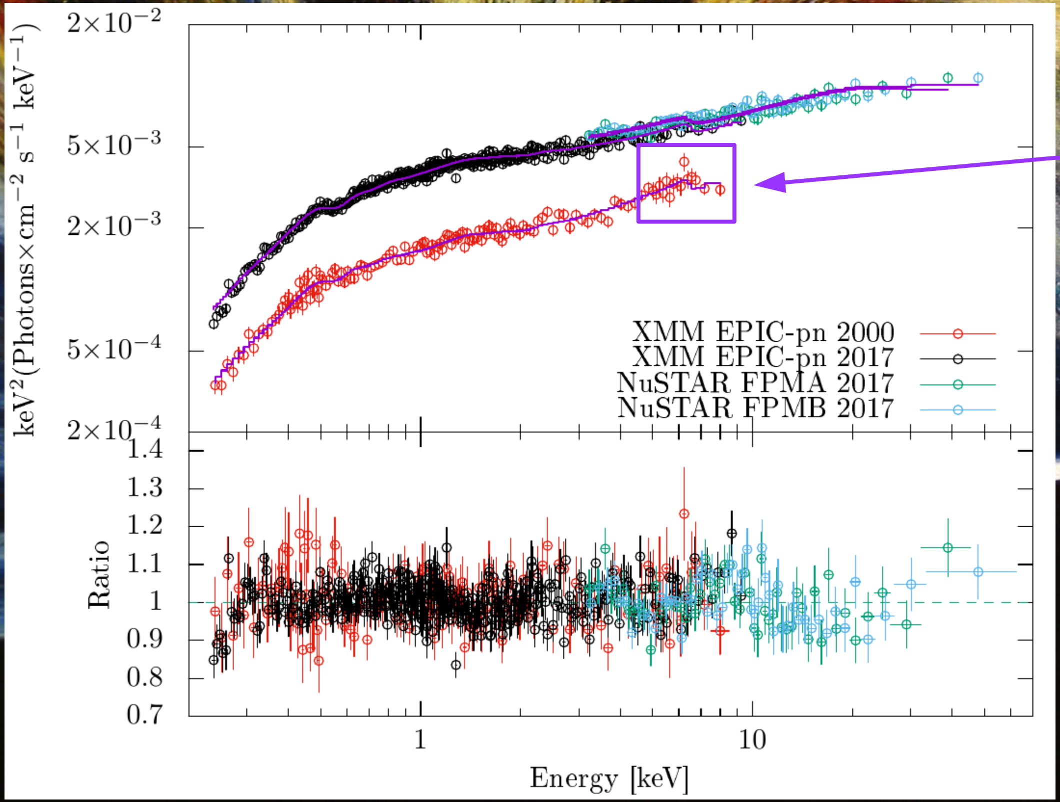

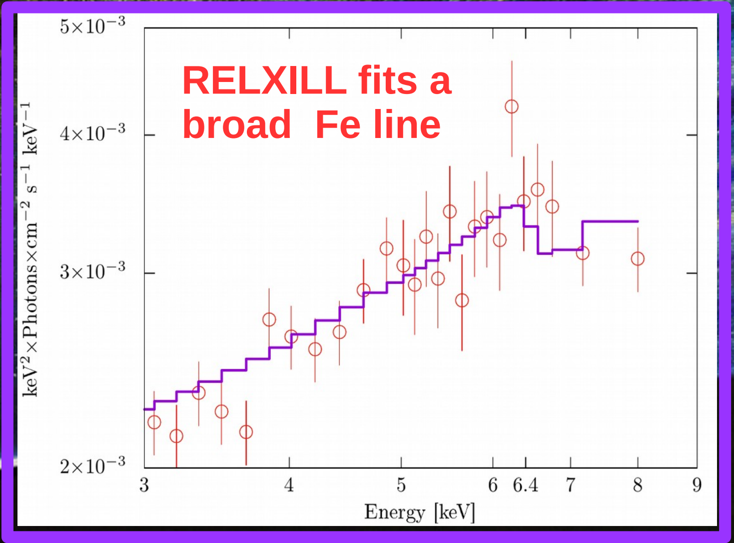

- $a > 0.98$.
- $\theta \sim 41^{o}$ (pegged to the limit)
- $R_{2000} \sim 2^{*} R_{2017}$

Relxill joint-fit results for different disk inclination

θ	a	Γ_{2000}	Γ_{2017}	log(ξ) (erg cm s^{-1})	A_{Fe}(solar)	R_{2000}	R_{2017}	χ^2/d.o.f
5°	$\geqslant 0.976$	$1.78^{+0.02}_{-0.03}$	$1.87^{+0.02}_{-0.01}$	$2.73^{+0.04}_{-0.01}$	$2.71^{+0.50}_{-0.52}$	$1.04^{+0.18}_{-0.16}$	$0.55^{+0.07}_{-0.05}$	777/599 (1.30)*
10°	$\geqslant 0.978$	$1.78^{+0.02}_{-0.03}$	$1.87^{+0.02}_{-0.01}$	$2.73^{+0.04}_{-0.03}$	$2.67^{+0.50}_{-0.52}$	$1.04^{+0.18}_{-0.12}$	0.56 ± 0.06	772/599 (1.29)*
22°	$\geqslant 0.983$	$1.78^{+0.02}_{-0.03}$	$1.87^{+0.02}_{-0.01}$	$2.73^{+0.03}_{-0.05}$	$2.47^{+0.51}_{-0.53}$	$1.07^{+0.18}_{-0.16}$	$0.56^{+0.06}_{-0.05}$	746.8/599 (1.25)*
35°	$\geqslant 0.986$	1.77 ± 0.03	$1.87^{+0.02}_{-0.01}$	$2.71^{+0.02}_{-0.05}$	$2.18^{+0.52}_{-0.56}$	$0.99^{+0.17}_{-0.14}$	$0.52^{+0.06}_{-0.05}$	710.4/599 (1.19)
40°	$\geqslant 0.988$	$1.77^{+0.02}_{-0.03}$	1.87 ± 0.01	$2.70^{+0.04}_{-0.05}$	$2.05^{+0.54}_{-0.56}$	$0.93^{+0.15}_{-0.14}$	0.49 ± 0.05	698.3/599 (1.17)
50°	$\geqslant 0.992$	1.76 ± 0.02	1.86 ± 0.01	$2.70^{+0.02}_{-0.06}$	$1.56^{+0.54}_{-0.57}$	$0.83^{+0.15}_{-0.11}$	$0.43^{+0.05}_{-0.04}$	691.3/599 (1.15)
60°	$\geqslant 0.993$	1.73 ± 0.02	1.84 ± 0.01	$2.70^{+0.02}_{-0.07}$	$1.19^{+0.65}_{-0.23}$	$0.56^{+0.08}_{-0.09}$	0.31 ± 0.03	693/599 (1.17)*
70°	$\geqslant 0.993$	1.85 ± 0.02	$1.92^{+0.02}_{-0.01}$	$1.30^{+0.08}_{-0.17}$	$0.72^{+0.23}_{-0.22}$	0.48 ± 0.07	$0.31^{+0.03}_{-0.04}$	708/599 (1.18)*
80°	$\leqslant 0.298$	$1.82^{+0.01}_{-0.02}$	1.89 ± 0.01	$1.11^{+0.20}_{-0.09}$	$0.64^{+0.26}_{-0.14}$	$0.29^{+0.01}_{-0.05}$	$0.18^{+0.03}_{-0.02}$	729.6/599 (1.22)*
55° ± 2°	$\geqslant 0.992$	1.74 ± 0.02	1.85 ± 0.01	$2.70^{+0.02}_{-0.05}$	$1.57^{+0.51}_{-0.46}$	$0.64^{+0.15}_{-0.09}$	$0.35^{+0.05}_{-0.03}$	685.2/598 (1.15)

Relxill joint-fit results for different disk inclination

θ	a	Γ_{2000}	Γ_{2017}	$\log(\xi)$ (erg cm s^{-1})	A_{Fe}(solar)	R_{2000}	R_{2017}	χ^2/d.o.f
5°	$\geqslant 0.976$	$1.78^{+0.02}_{-0.03}$	$1.87^{+0.02}_{-0.01}$	$2.73^{+0.04}_{-0.01}$	$2.71^{+0.50}_{-0.52}$	$1.04^{+0.18}_{-0.16}$	$0.55^{+0.07}_{-0.05}$	777/599 (1.30)*
10°	$\geqslant 0.978$	$1.78^{+0.02}_{-0.03}$	$1.87^{+0.02}_{-0.01}$	$2.73^{+0.04}_{-0.03}$	$2.67^{+0.50}_{-0.52}$	$1.04^{+0.18}_{-0.12}$	0.56±0.06	772/599 (1.29)*
22°	$\geqslant 0.983$	$1.78^{+0.02}_{-0.03}$	$1.87^{+0.02}_{-0.01}$	$2.73^{+0.03}_{-0.05}$	$2.47^{+0.51}_{-0.53}$	$1.07^{+0.18}_{-0.16}$	$0.56^{+0.06}_{-0.05}$	746.8/599 (1.25)*
35°	$\geqslant 0.986$	1.77±0.03	$1.87^{+0.02}_{-0.01}$	$2.71^{+0.02}_{-0.05}$	$2.18^{+0.52}_{-0.56}$	$0.99^{+0.17}_{-0.14}$	$0.52^{+0.06}_{-0.05}$	710.4/599 (1.19)
40°	$\geqslant 0.988$	$1.77^{+0.02}_{-0.03}$	1.87±0.01	$2.70^{+0.04}_{-0.05}$	$2.05^{+0.54}_{-0.56}$	$0.93^{+0.15}_{-0.14}$	0.49±0.05	698.3/599 (1.17)
50°	$\geqslant 0.992$	1.76±0.02	1.86±0.01	$2.70^{+0.02}_{-0.06}$	$1.56^{+0.54}_{-0.57}$	$0.83^{+0.15}_{-0.11}$	$0.43^{+0.05}_{-0.04}$	691.3/599 (1.15)
60°	$\geqslant 0.993$	1.73±0.02	1.84± 0.01	$2.70^{+0.02}_{-0.07}$	$1.19^{+0.65}_{-0.23}$	$0.56^{+0.08}_{-0.09}$	0.31±0.03	693/599 (1.17)*
70°	$\geqslant 0.993$	1.85±0.02	$1.92^{+0.02}_{-0.01}$	$1.30^{+0.08}_{-0.17}$	$0.72^{+0.23}_{-0.22}$	0.48±0.07	$0.31^{+0.03}_{-0.04}$	708/599 (1.18)*
80°	≤ 0.298	$1.82^{+0.01}_{-0.02}$	1.89±0.01	$1.11^{+0.20}_{-0.09}$	$0.64^{+0.26}_{-0.14}$	$0.29^{+0.01}_{-0.05}$	$0.18^{+0.03}_{-0.02}$	729.6/599 (1.22)*
55° ± 2°	$\geqslant 0.992$	1.74±0.02	1.85±0.01	$2.70^{+0.02}_{-0.05}$	$1.57^{+0.51}_{-0.46}$	$0.64^{+0.15}_{-0.09}$	$0.35^{+0.05}_{-0.03}$	685.2/598 (1.15)

Chamani+2019, submitted to A&A

Summary and discussion

- **Soft -excess observed in the XMM 2000 and 2017 data sets.**
- **A promiment Fe Kα line detected in the XMM 2000 data set (Salvi + 2002; Piconcelli + 2005; Gonzalez + 2018).**
- **The relxill fits favour fast rotating black hole *a*~0.9 in III Zw 2, but it has a weak jet!.**
- **High spins does not produce necessarily powerful jets.**
- **Do III Zw 2 jet is below the MAD level? We will measure the magnetic flux with VLBI observations (in collaboration with Hada-san).**


Thanks for your attention!